Progress In Electromagnetics Research, Vol. 132, 215–232, 2012

SUB-MILLIMETER WAVE FREQUENCY SCANNING 8 × 1 ANTENNA ARRAY

R. Camblor Diaz*, S. Ver Hoeye, C. Vázquez, G. Hotopan, M. Fernández, and F. Las Heras

Area of Signal Theory and Communications, Department of Electrical Engineering, University of Oviedo, Campus de Viesques, Edificio Polivalente s/n, mod. 8, 1a planta E-33203, Gijón/Xixón, Spain

Abstract—In this work, a sub-millimeter wave frequency scanning 8×1 element antenna array is presented for its use in a terahertz imaging system operating in the 220–330 GHz frequency band. The antenna array is formed by eight open ended waveguides, a phase-shifting network implemented with WR-3 rectangular waveguides and a power divider. Dielectric rods are used to improve the radiation patterns at large beam-steering angles. Prototypes of antenna arrays with and without the dielectric rods have been manufactured and experimentally characterized. A beam-steering range greater than 40° has been obtained for a frequency sweep between 270 GHz and 330 GHz.

1. INTRODUCTION

During the last decade, a large research effort has been dedicated to the development of sub-millimeter wave technology (300 GHz–3 THz), due to the large number of potential applications in different areas, such as terahertz imaging and sensing [1–11], wireless communications [12], radio-astronomy [13], fast measurement systems [14], non-destructive material analysis [15–18], or non-ionizing diagnosis [19–22], among others.

Many of these applications require THz active imaging systems with a reduced image acquisition time. In these systems [23, 24], the scene is illuminated with millimeter wave, sub-millimeter wave, or terahertz radiation and the amount of power reflected by or passed through different targets is measured. Multiple types of

Received 23 July 2012, Accepted 24 August 2012, Scheduled 27 September 2012

* Corresponding author: Rene Camblor Diaz (rcamblor@tsc.uniovi.es).

illuminations of the object under investigation can be chosen, using single frequency [25], multi-frequency [26, 27] or Ultra Wide Band (UWB) signals [28].

Different measurement setups have been proposed, based on mechanically rotating mirrors, combined with a linear movement of the probe [23], a rotary scanner with variable radius [29], etc. The measurement equipment can be reduced to a minimum when using a Vector Network Analyzer (VNA), along with auxiliary circuitry [27]. An interesting option is the use of a receiving probe based on a frequency scanning antenna array [30–33], which can be directly controlled by the VNA, as it provides the required steering behavior, without further increasing the complexity of the measurement setup.

For the realization of antenna arrays at millimeter and sub-millimeter wave frequencies, different technologies and topologies have been proposed for the implementation of the radiating elements and their corresponding feeding network, based on either microstrip technology [30–35] or waveguide structures [36, 37].

In this work, a Sub-Millimeter Wave Frequency Scanning Antenna Array is proposed for its application in an imaging setup as depicted in Fig. 1. The object under investigation, illuminated by a frequency scanning antenna array with a main lobe that can be steered in the vertical plane, is placed on an azimuthal positioner and progressively rotated to evaluate the response for multiple incidence angles. A mildly directive horn antenna is applied to receive uniformly the reflected power from different illuminated vertical segments of the target.

A rectangular waveguide based structure is presented for the implementation of the power divider and the phase shifting network. Open ended waveguides are used as radiating elements. In order

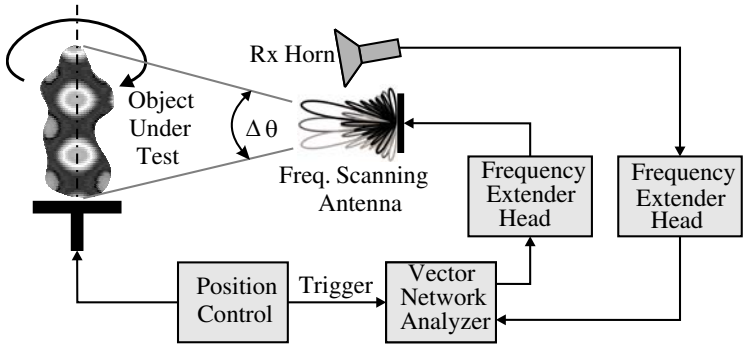

Figure 1. Imaging setup based on the use of a terahertz frequency scanning antenna array.

to reduce the sidelobe level in the radiation patterns at large beam steering angles, dielectric rods have been designed for their insertion in the open ended waveguides.

The paper is organized as follows. In Section 2, the topology and design process of the different elements that compose the sub-millimeter wave frequency scanning antenna array are described. Section 3 is dedicated to the analysis of the frequency scanning behavior of the antenna. The manufacturing process and the results of the experimental characterization of the beam steering behavior of the antenna are presented in Section 4.

2. TOPOLOGY AND DESIGN OF THE FREQUENCY SCANNING ANTENNA

2.1. Topology

The topology of the Sub-Millimeter Wave Frequency Scanning Antenna Array is shown in Fig. 2. The antenna consists of three different parts: A power divider delivering the input power to a WR-3 waveguide phase-shifting network, which feeds an 8×1 antenna array composed by eight WR-3 waveguide apertures (with or without dielectric rods).

The antenna is designed to be implemented using metallic WR-3 rectangular waveguide [(internal dimensions 0.864 mm $\times$ 0.432 mm (depth $\times$ width)) based structures with frequency range between 220–330 GHz. The structural details (bends, dividers, etc.) are all

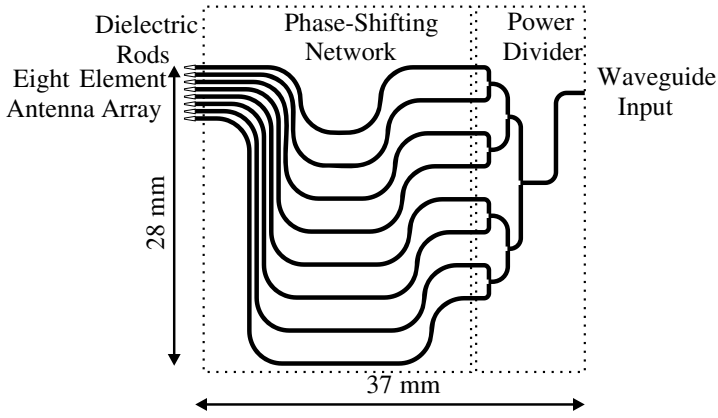

Figure 2. Topology of the frequency scanning antenna array with inclusion of a power divider, phase-shifting network, the 8×1 radiating open ended waveguide apertures and the dielectric rods.

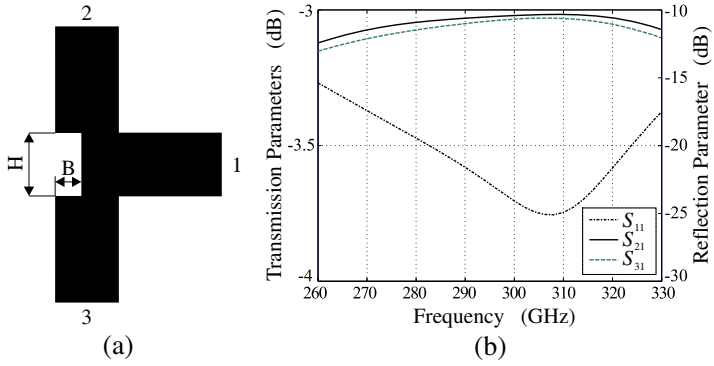

Figure 3. Power divider element: (a) design, (b) simulated transmission and reflection parameters.

introduced in the E-plane, i.e., the depth of all elements of the design is constant (0.864 mm). The system has been designed with the aid of the Ansys HFSS software.

In order to facilitate the alignment of the antenna during the mounting and measurement processes, the waveguide input at the beginning of the power divider is situated at the center of the 8×1 antenna array.

2.2. Power Divider

The power dividing network of Fig. 2 is implemented in three stages using the divider element depicted in Fig. 3(a). The depth of the element is 0.864 mm, while $B = 0.177$ mm and $H = 0.425$ mm. The simulated transmission and reflection parameters of this single power divider element are shown in Fig. 3(b).

The simulated behavior of the complete power divider as depicted in Fig. 4(a) is shown in Fig. 4(b). The power divider is matched over the whole frequency range of operation, and the overall signal losses from the input (port 1) port towards any output port (port 2–port 9) are below 0.7 dB, see Fig. 4(b).

2.3. Phase-shifting Network

The phase shifting network is implemented with WR-3 rectangular waveguide based transmission line segments of different lengths. The phase shift $\Delta\phi$, undergone by an electromagnetic wave propagating through a transmission line of length L, is known to be given by

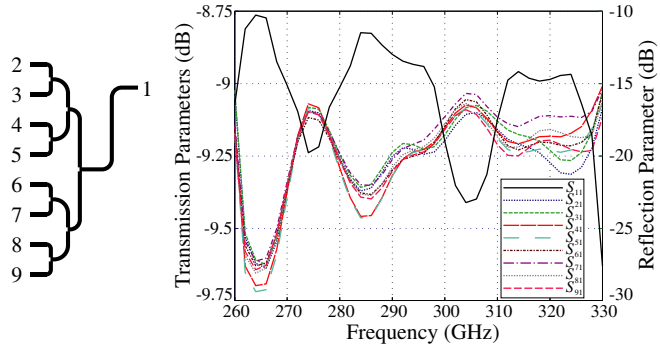

Figure 4. Complete power divider: (a) design, (b) simulated transmission and reflection parameters.

$\Delta\phi = -2\pi L/\lambda_g = -2\pi f L/\nu_p$, where f is the operating frequency and ν_p is the propagation velocity in the waveguide.

For a fixed transmission line length L, the phase shift $\Delta\phi$ is linearly dependent on the operation frequency. For the main beam to be pointed at the boresight direction at the centre frequency f_0, the difference in electrical length between the feeding line of the consecutive antenna elements must be an integer multiple ($N \in \mathbb{N}$) of the guided wavelength λ_g at that frequency, $\Delta L = N\lambda_g$. In this work, in order to achieve the required steering range of, at least, $\Delta\theta = 40°$, $N = 2$ has been chosen.

The same radius has been used for all the bends in the phase-shifting network, and ΔL is only introduced in straight sections, thus avoiding accumulated phase-shifting errors in the different branches of the network, that might be introduced in the manufacturing process.

The phase shift differences between the output ports $\Delta\phi_n = \phi_{Sn1} - \phi_{S21}$ are shown in Fig. 5. For the design of the structure, a central frequency $f_0 = 300\,\text{GHz}$ is considered. A progressive phase shift distribution is obtained over the whole frequency range.

2.4. Antenna Radiating Elements

The 8×1 antenna array is composed by eight radiating open ended WR-3 waveguides, stacked in the direction of the E-plane, with a distance of 1 mm between consecutive elements.

An improved version of the antenna is implemented as well, in which the waveguide apertures are ended in dielectric rods, designed to lower the high sidelobes in the radiating patterns, which arise at

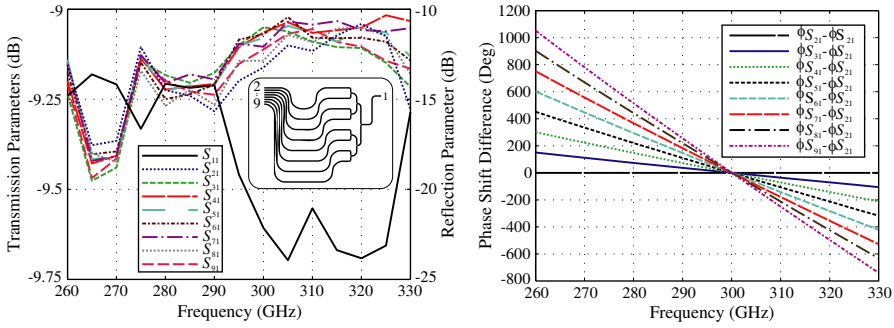

(a) (b)

Figure 5. Phase shifting network: (a) simulated transmission and reflection parameters, (b) simulated phase shift differences between output ports $\Delta\phi_n = \phi_{Sn1} - \phi_{S21}$.

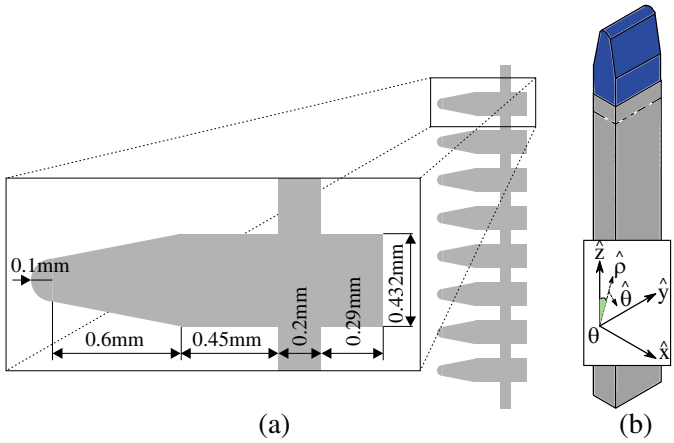

(a) (b)

Figure 6. Design of the dielectric rods in a methacrylate sheet with a 0.864 mm thickness. (a) Array of 8 connected dielectric rods, (b) single rod inserted in an open ended rectangular waveguide.

large beam steering angles. Fig. 6 shows the design of the dielectric rods, to be micromachined out of a methacrylate sheet with a thickness of 0.864 mm.

The eight rods are connected by a thin bridge with a height of 0.2 mm, in order to facilitate their assembly (Fig. 6(a)), and end in a 0.29 mm long protrusion which is inserted inside the waveguide apertures of the antenna array (Fig. 6(b)).

The simulated reflection parameters for a single waveguide and of the complete frequency scanning antenna array, with and without

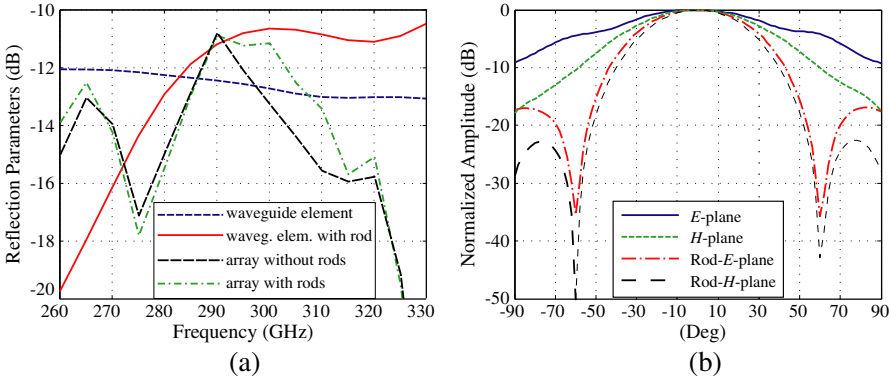

Figure 7. Simulated behavior of the waveguides with and without dielectric rods: (a) reflection parameters for a single waveguide and of the complete antenna, and (b) radiation pattern of an open ended single waveguide aperture, with and without rod.

dielectric rods, are shown in Fig. 7(a). The radiation patterns of the open ended single waveguide aperture with and without rod are shown in Fig. 7(b). A permittivity $\varepsilon_r = 2.66$ has been considered for the methacrylate.

3. FREQUENCY SCANNING BEHAVIOR

The simulated frequency scanning behavior of both antenna arrays, with and without dielectric rods, is presented in Fig. 8, showing the radiation patterns corresponding to the frequencies: 270 GHz, 285 GHz, 295 GHz, 305 GHz, 315 GHz, and 330 GHz. As can be observed in Fig. 8, the obtained steering range $\Delta\theta$ is greater than 40 degrees.

The effect of the dielectric rods in the radiation patterns at large beam steering angles can be clearly seen in Fig. 8(f), where a strong reduction of the high sidelobe level is obtained at $\theta = -65°$, when the main lobe is at $\theta = 20°$ approximately.

The simulated H-plane radiation pattern of the frequency scanning antenna arrays operating at the central frequency $f_0 = 300$ GHz is shown in Fig. 9.

As can be seen from Fig. 9, the presence of the dielectric rods leads also to an improvement of the directivity of the radiation pattern in the H-plane.

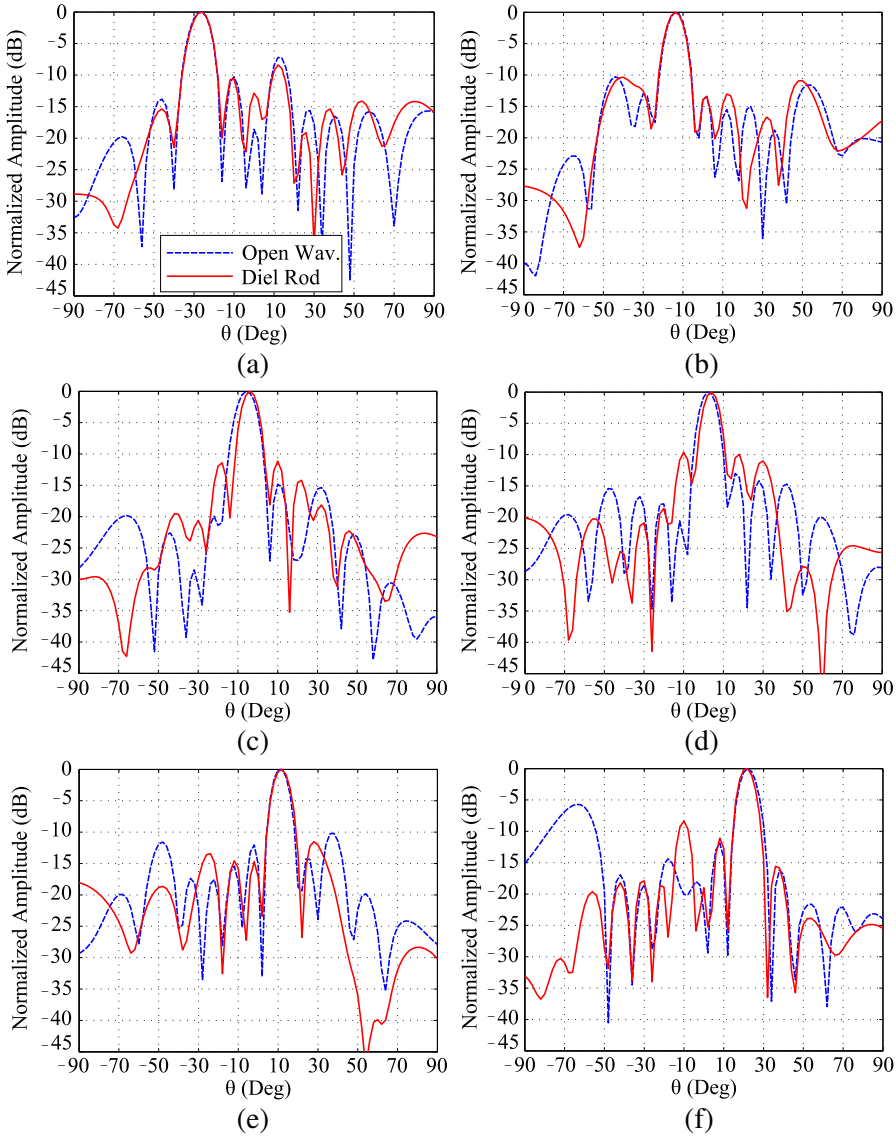

Figure 8. Simulated frequency scanning behavior of the antenna array without (dashed line) and with (continuous line) dielectric rods at (a) 270 GHz, (b) 285 GHz, (c) 295 GHz, (d) 305 GHz, (e) 315 GHz, (f) 330 GHz.

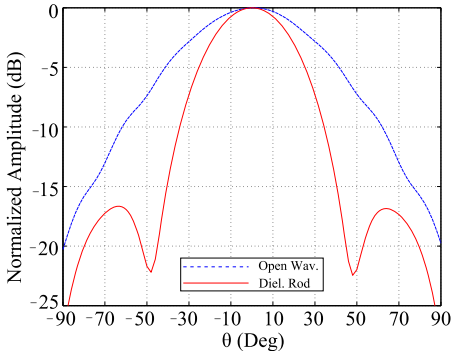

Figure 9. Simulated H-plane radiation patterns of the frequency scanning antenna array without (dashed line) and with (continuous line) dielectric rods at 300 GHz.

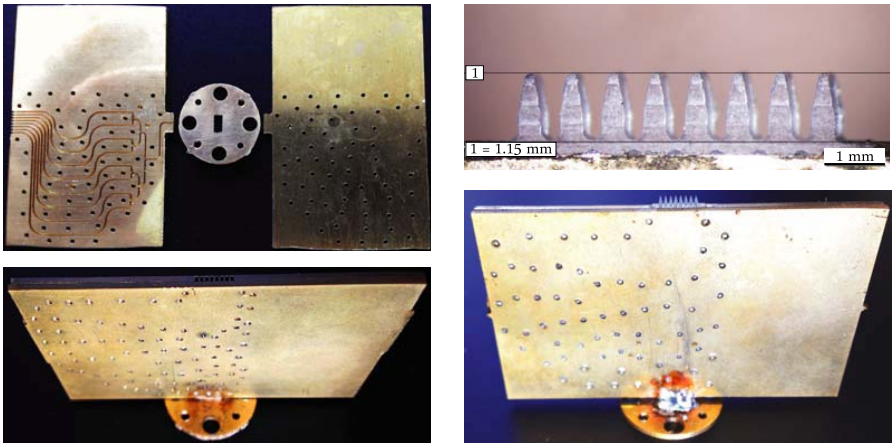

Figure 10. Manufactured frequency scanning antenna arrays: (a) Elements of the antenna without dielectric rods. (b) Dielectric rods and corresponding antenna array.

4. EXPERIMENTAL RESULTS

4.1. Manufactured Prototypes

The whole structure represented in Fig. 2 (without dielectric rods) has been manufactured in brass metal with a micromechanical milling process using end-mill tools with diameters of 0.25 mm and 0.4 mm. The full depth (0.864 mm) of the structure is milled in a first 1 mm thick brass metal sheet, corresponding to the largest WR-

Figure 11. Cylindrical antenna measurement setup.

3 rectangular waveguide dimension (Fig. 10(a)). The rectangular waveguide structure is closed by a second brass metal sheet, which has been attached to it using microscrews.

In order to be able to measure the frequency scanning antenna array using VDI-frequency extender heads, a WR-3 standard flange has been manufactured and soldered to the waveguide input (Fig. 10(a)).

For the second version of the frequency scanning antenna array, the 8×1 group of dielectric rods has been micromachined in a methacrylate sheet, which was previously reduced in thickness to the desired 0.864 mm, using a milling process.

Figures 10(a) and 10(b) show the different elements of the manufactured prototypes of the 8×1 frequency scanning antenna array, respectively without and with dielectric rods.

4.2. Characterization with Cylindrical Measurement Setup

The manufactured prototypes have been tested firstly using the cylindrical measurement setup depicted in Fig. 11, composed by an Agilent PNA-X vector network analyzer, two frequency extender heads operating in the 220–330 GHz range from Virginia Diodes and a rotation plate.

The sub-millimeter wave signal feeding the transmitting antenna is generated by a Tx/Rx Frequency Extender Head while the signal received by the Frequency Scanning Antenna Array is detected with a Rx Frequency Extender Head (Fig. 11). The prototype of Frequency Scanning Antenna Array under test together with the Rx Frequency Extender Head is mounted on the rotation plate.

The measured reflection parameters of the two prototypes are shown in Fig. 12.

The radiation patterns of the Frequency Scanning Antenna Array at different operation frequencies have been obtained by measuring, for each rotation angle θ, the received power in the whole frequency range between 260 GHz and 330 GHz. The distance between the antenna under test and the probe antenna is 200 mm, to fulfil the far-field

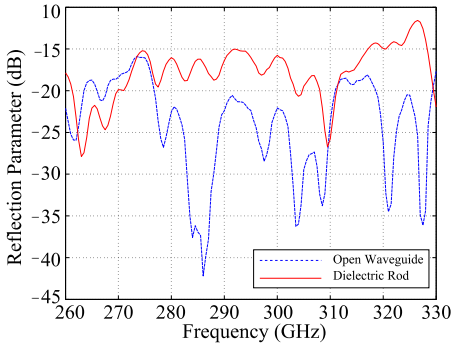

Figure 12. Reflection parameters of the frequency scanning antenna arrays without (dashed line) and with (continuous line) dielectric rods.

Table 1. 10 dB E-plane beamwidth comparison.

Frequency (GHz)		270	285	295	305	315	330
Simulation	Rod (°)	17.8	16	14.4	14.2	14.5	14
	Open Wav. (°)	17.8	16	17.3	15	13.8	15
Measurement	Rod (°)	21.5	16.3	15.9	16.7	17.5	16.1
	Open Wav. (°)	24.1	16.5	15.9	16.7	17.1	16.7

condition. Once all the measurement data has been obtained for the different angles θ between $-70°$ and $70°$ (with steps of $0.5°$), the diagrams corresponding to the frequencies 270 GHz, 285 GHz, 295 GHz, 305 GHz, 315 GHz, and 330 GHz have been composed (Fig. 13).

As can be observed from Fig. 13(f), the lowering of high sidelobes predicted by the simulations, in the radiation patterns corresponding to high beam steering angles, is also found in the measured frequency scanning behavior of the antenna array with dielectric rods.

The measured H-plane radiation patterns of both prototypes are represented in Fig. 14. Again, a good agreement is observed between simulated results and measurements.

Table 1 shows a comparison between the 10 dB E-plane beamwidth for simulations and measurements with and without dielectric rods at different frequencies.

The differences between the 10 dB H-plane beamwidth simulations and measurements with and without dielectric rods can be seen in Table 2. Beamwidth reduction with rods is clearly seen both in simulations and measurements.

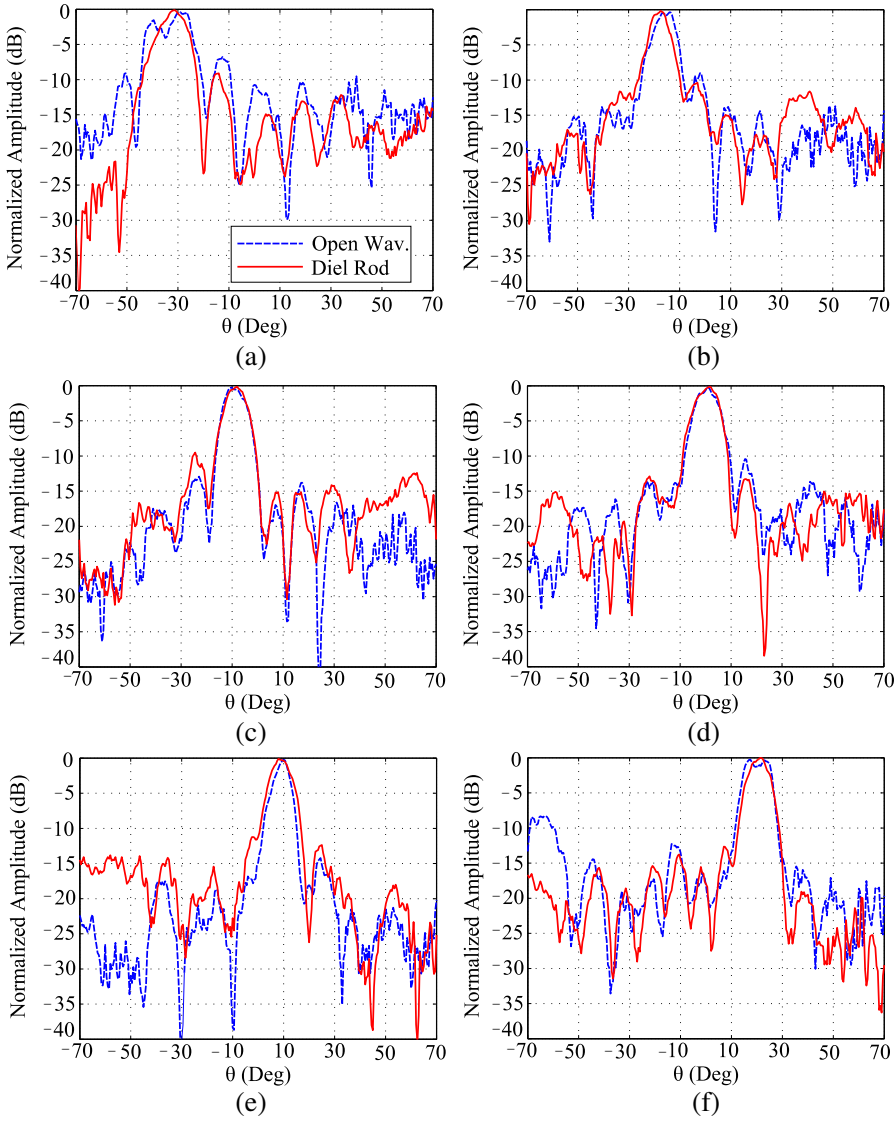

Figure 13. Measured radiation patterns of the antenna array without (dashed line) and with (continuous line) dielectric rods at (a) 270 GHz, (b) 285 GHz, (c) 295 GHz, (d) 305 GHz, (e) 315 GHz, (f) 330 GHz.

4.3. Characterization with *XY* Scanner Setup

A second experimental characterization of the frequency scanning behavior of the frequency scanning antenna with dielectric rods has

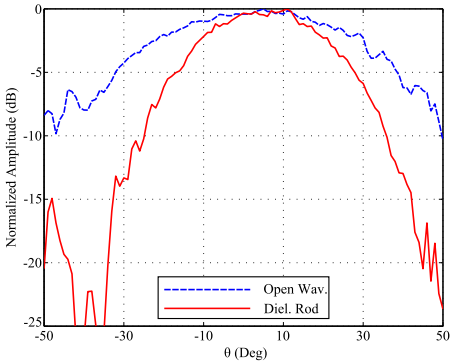

Figure 14. Measured H-plane radiation patterns of the frequency scanning antenna array without (dashed line) and with (continuous) dielectric rods at 300 GHz.

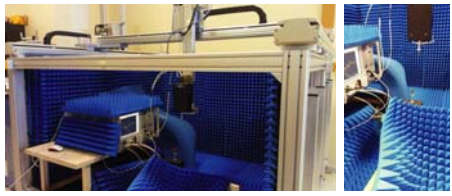

Figure 15. XYZ scanner used in the xy antenna measurement setup.

Table 2. 10 dB H-plane beamwidth comparison at 300 GHz.

Simulation	Rod (°)	68.7
	Open Wav. (°)	123.7
Measurement	Rod (°)	60.8
	Open Wav. (°)	98.8

been realized using the XY measurement setup shown in Fig. 15. As in the cylindrical measurement setup, a vector network analyzer and two frequency extender heads operating in the 220–330 GHz are used. In this setup, the antenna prototype was mounted on the transmitting frequency extender head, which was maintained in a fixed position, while the receiving antenna, was mounted on the detecting frequency extender head, which was moved by the scanning arm of the xy-table.

In order to guarantee a far field measurement setup, the antenna is situated, by means of the z-movement of the table, at a distance of 25 cm. The radiation patterns are scanned at that distance in an area of 30 cm × 30 cm, which corresponds to an approximate angular variation in the x and y direction of 31°. The step used in the x-and y-direction has been 4 mm, and the received power has been measured

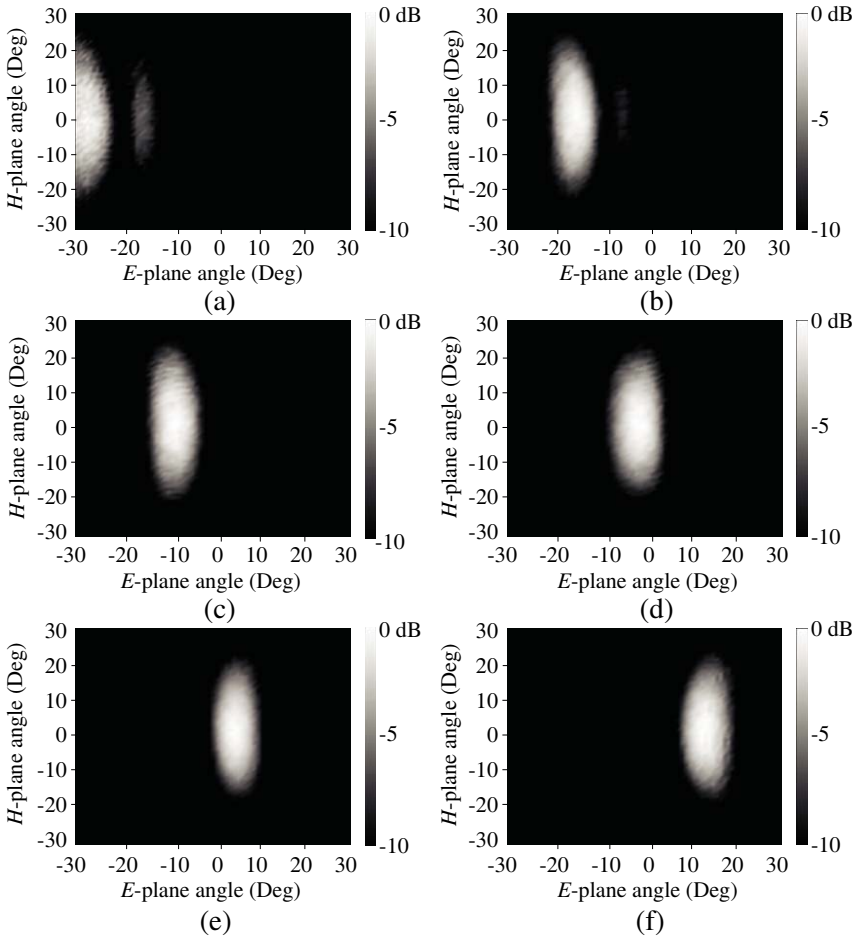

Figure 16. Measured radiation patterns of the antenna array with dielectric rods at (a) 270 GHz, (b) 285 GHz, (c) 295 GHz, (d) 305 GHz, (e) 315 GHz, (f) 330 GHz.

for each position in the 270–330 GHz frequency range with a step of 5 GHz. The radiation patterns are composed by representing, for each particular frequency, the received power at all x-y positions.

The radiation patterns at 270 GHz, 285 GHz, 295 GHz, 305 GHz, 315 GHz and 330 GHz are shown in Fig. 16.

Table 3 shows a comparison between the maximum of the radiation diagram measured using the XY setup for each frequency. The values are normalized to the absolute maximum, which takes place at 315 GHz.

Table 3. Normalized variation of the maximum of the measured radiation diagram in frequency.

Frequency (GHz)	270	285	295	305	315	330
Normalized Value (dB)	−5.9	−4.7	-3.8	−2.3	0	−0.47

5. CONCLUSIONS

An 8×1 frequency scanning antenna array design has been presented for its operation in the 270–330 GHz frequency band. The antenna and the corresponding feeding network have been designed in WR-3 rectangular waveguide structures and implemented in brass metal using mechanical micro-milling facilities. A reduction of the sidelobe level appearing when operating at large beam steering angles has been achieved through the insertion of dielectric rods at the end of the radiating open ended waveguides of the antenna array. The two antenna prototypes have been measured using both a cylindrical and a XY scanner setup. The obtained beam steering capabilities when varying the operation frequency in the 270–330 GHz band have exceeded successfully the expected range of 40°.

ACKNOWLEDGMENT

This work has been supported by the "Ministerio de Ciencia e Innovación of Spain/FEDER" and "FEDER", under projects IPT-2011-0951-390000 (TECNIGRAF), TEC2011-24491 (ISCAT), CONSOLIDER-INGENIO CSD2008-00068 (TERASENSENSE) and grant AP2009-0438, by the "Gobierno del Principado de Asturias (PCTI)/FEDER-FSE" under projects EQUIP08-06, FC09-COF09-12, EQUIP10-31 and PC10-06, grant BP10-031 and by "Cátedra Telefónica — Universidad de Oviedo".

REFERENCES

1. Hadjiloucas, S., et al., "Measurement of leaf water content using terahertz radiation," *IEEE Transactions on Microwave Theory and Techniques*, Vol. 47, No. 2, 142–149, 1999.
2. Oka, S., H. Togo, N. Kukutsu, and T. Nagatsuma, "Latest trends in millimeter-wave imaging technology," *Progress In Electromagnetics Research Letters*, Vol. 1, 197–204, 2008.
3. Dickinson, J. C., et al., "Terahertz imaging of subjects with concealed weapons," *Proceedings of SPIE*, Vol. 6212, 2006.

4. Cai, M. and E. P. Li, "A novel terahertz sensing device comprising of a parabolic reflective surface and a bi-conical structure," *Progress In Electromagnetics Research*, Vol. 97, 61–73, 2009.
5. Matvejev, V., C. De Tandt, W. Ranson, J. Stiens, R. Vounckx, and D. Mangelings, "Integrated waveguide structure for highly sensitive THz spectroscopy of nano-liter liquids in capillary tubes," *Progress In Electromagnetics Research*, Vol. 121, 89–101, 2011.
6. Qi, F., V. Tavakol, D. Schreurs, and B. K. J. C. Nauwelaers, "Limitations of approximations towards Fourier optics for indoor active millimeter wave imaging systems," *Progress In Electromagnetics Research*, Vol. 109, 245–262, 2010.
7. Yeom, S., D. Lee, H. Lee, J. Son, and V. P. Guschin, "Distance estimation of concealed objects with stereoscopic passive millimeter-wave imaging," *Progress In Electromagnetics Research*, Vol. 115, 399–407, 2011.
8. Hu, T., Z. Xiao, J. Xu, and L. Wu, "Effects of reverse radiation noise on millimeter-wave radiometric imaging at short range," *Progress In Electromagnetics Research M*, Vol. 21, 177–188, 2011.
9. Demirci, S., H. Cetinkaya, E. Yigit, C. Ozdemir, and A. A. Vertiy, "A study on millimeter-wave imaging of concealed objects: Application using back-projection algorithm," *Progress In Electromagnetics Research*, Vol. 128, 457–477, 2012.
10. Zhu, B., J. Stiens, V. Matvejev, and R. Vounckx, "Inexpensive and easy fabrication of multimode tapered dielectric circular probes at millimeter wave frequencies," *Progress In Electromagnetics Research*, Vol. 126, 237–254, 2012.
11. Hu, B. B. and M. C. Nuss, "Imaging with terahertz waves," *Optical Letters*, Vol. 20, No. 16, 1716–1719, 1995.
12. Hirata, A., M. Harada, and T. Nagatsuma, "120-GHz wireless link using photonic techniques for generation, modulation, emission of millimeter-wave signals," *Journal of Lightwave Technology*, Vol. 21, No. 10, 2145–2153, 2003.
13. Payne, J., B. Shillue, and A. Vaccari, "Photonic techniques for use on the Atacama large millimeter array," *MWP'99 Techn. Digest*, 105–108, Nov. 1999.
14. Wu, Q. and X. C. Zhang, "Free-space electro-optics sampling of midinfrared pulses," *Appl. Phys. Lett.*, Vol. 71, No. 10, 1285–1287, 1997.
15. Nuss, M. C. and J. Orenstein, "Terahertz time-domain spectroscopy," *Millimeter and Submillimeter Wave Spectroscopy*

in Solids, J. Grner (ed.), Ch. 2, 7–109, Springer, Berlin, Germany, 1998.

16. Lucyszyn, S. and Y. Zhou, "Engineering approach to modeling frequency dispersion within normal metals at room temperature for THz applications," *Progress In Electromagnetics Research*, Vol. 101, 257–275, 2010.
17. Lucyszyn, S. and Y. Zhou, "Characterising room temperature THz metal shielding using the engineering approach," *Progress In Electromagnetics Research*, Vol. 103, 17–31, 2010.
18. Huang, F., et al., "Terahertz study of 1, 3, 5-trinito-s-triazine by time-domain and Fourier transform infrared spectroscopy," *Applied Physics Letters*, Vol. 85, 5535–5537, 2004.
19. Heh, D. Y. and E. L. Tan, "Modeling the interaction of terahertz pulse with healthy skin and basal cell carcinoma using the unconditionally stable fundamental ADI-FDTD method," *Progress In Electromagnetics Research B*, Vol. 37, 365–386, 2012.
20. Hassan, A. and M. El-Shenawee, "Review of electromagnetic techniques for breast cancer detection," *IEEE Reviews in Biomedical Engineering*, Vol. 4, 103–118, 2011.
21. Laurette, S., A. Treizebre, N.-E. Bourzgui, and B. Bocquet, "Terahertz interferometer for integrated Goubau-line waveguides," *Progress In Electromagnetics Research Letters*, Vol. 30, 49–58, 2012.
22. Treizebre, A., S. Laurette, Y. Xu, R. G. Bosisio, and B. Bocquet, "Thz power divider circuits on planar Goubau lines (PGLS)," *Progress In Electromagnetics Research C*, Vol. 26, 219–228, 2012.
23. Tran, H., et al., "A fast scanning w-band system for advanced millimetre-wave short range imaging applications," *3rd European Radar Conference, EURAD 2006*, 146–149, 2006.
24. Sheen, D., et al., "Three-dimensional millimeter-wave imaging for concealed weapon detection," *IEEE Transactions on Microwave Theory and Techniques*, Vol. 49, No. 9, 1581–1592, Sep. 2001.
25. Chu, T.-H., et al., "Microwave diversity imaging of perfectly conducting object in the close near-field region," *Antennas and Propagation Society International Symposium*, 82–85, Jun. 1989.
26. Lin, D. and T. Chu, "Bistatic frequency-swept microwave imaging: Principle, methodology and experimental results," *IEEE Transactions on Microwave Theory and Techniques*, Vol. 41, No. 5, 855–861, May 1993.
27. Tseng, C.-H., et al., "An effective usage of vector network analyzer for microwave imaging," *IEEE Transactions on Microwave Theory*

and Techniques, Vol. 53, No. 9, 2884–2891, Sep. 2005.

28. Abbosh, A., "Compact antenna for microwave imaging systems," *Cairo International Biomedical Engineering Conference, CIBEC*, 1–4, Dec. 2008.
29. Ghasr, M., et al. "Rapid rotary scanner and portable coherent wideband Q-band transceiver for high-resolution millimeter-wave imaging applications," *IEEE Transactions on Instrumentation and Measurement*, Vol. 60, No. 1, 186–197, Dec. 2008.
30. Vázquez, C., S. Ver Hoeye, M. Fernández, L. F. Herrán, and F. Las Heras, "Frequency scanning probe for microwave imaging," *IEEE Antennas and Propagation Society International Symposium, APSURSI*, 1–4, Dec. 2010.
31. Camblor, R., S. Ver Hoeye, G. Hotopan, C. Vázquez, M. Fernández, and F. Las Heras, "Design of a submillimeter microstrip array for beam-scanning applications," *The 35th International Conference on Infrared, Millimeter and THz Waves IRMMW-THz*, 1–3, Rome, 2010.
32. Camblor, R., S. Ver Hoeye, G. Hotopan, and C. Vázquez, G. Hotopan, M. Fernández, and F. Las Heras, "Frequency scanning array composed of antipodal linearly tapered slot antennas," *Journal of Electromagnetic Waves and Applications*, Vol. 26, No. 4, 468–479, 2012.
33. Álvarez, Y., C. García Vázquez, S. Ver Hoeye, and F. Las Heras, "Measurement setup for imaging applications using frequency scanning illumination," *IEEE Transactions on Instrumentation and Measurement*, Vol. PP, No. 99, 1–10, 2012.
34. Peters, F. D. L., B. Boukari, S. O. Tatu, and T. A. Denidni, "77 GHz Millimeter wave antenna array with Wilkinson divider feeding network," *Progress In Electromagnetics Research Letters*, Vol. 9, 193–199, 2009.
35. Peters, F. D. L., D. Hammou, S. O. Tatu, and T. A. Denidni, "Modified millimeter-wave Wilkinson power divider for antenna feeding networks," *Progress In Electromagnetics Research Letters*, Vol. 17, 11–18, 2010.
36. Dou, W.-B., H. F. Meng, B. Ni, Z.-X. Wang, and F. Yang, "Scanning antenna at THz band based on quasi-optical techniques," *Progress In Electromagnetics Research*, Vol. 108, 343–359, 2010.
37. Cullens, E. D., L. Ranzani, K. J. Vanhille, E. N. Grossman, E. Ehsan, and Z. Popovic, "Micro-fabricated 130–180 GHz frequency scanning waveguide arrays," *IEEE Transactions on Antennas and Propagation*, 2012.